REPORT

www.the-innovation.org

Rational multivalency construction enables bactericidal effect amplification and dynamic biomaterial design

Xu Chen,[1] Xinrui Li,[1] Wenbo He,[1] Miao Wang,[1] Ang Gao,[2] Liping Tong,[2,*] Shun Guo,[1] Huaiyu Wang,[2,*] and Guoqing Pan[1,*]

*Correspondence: lp.tong@siat.ac.cn (L.T.); hy.wang1@siat.ac.cn (H.W.); panguoqing@ujs.edu.cn (G.P.)

Received: March 17, 2023; Accepted: July 10, 2023; Published Online: July 13, 2023; https://doi.org/10.1016/j.xinn.2023.100483

GRAPHICAL ABSTRACT

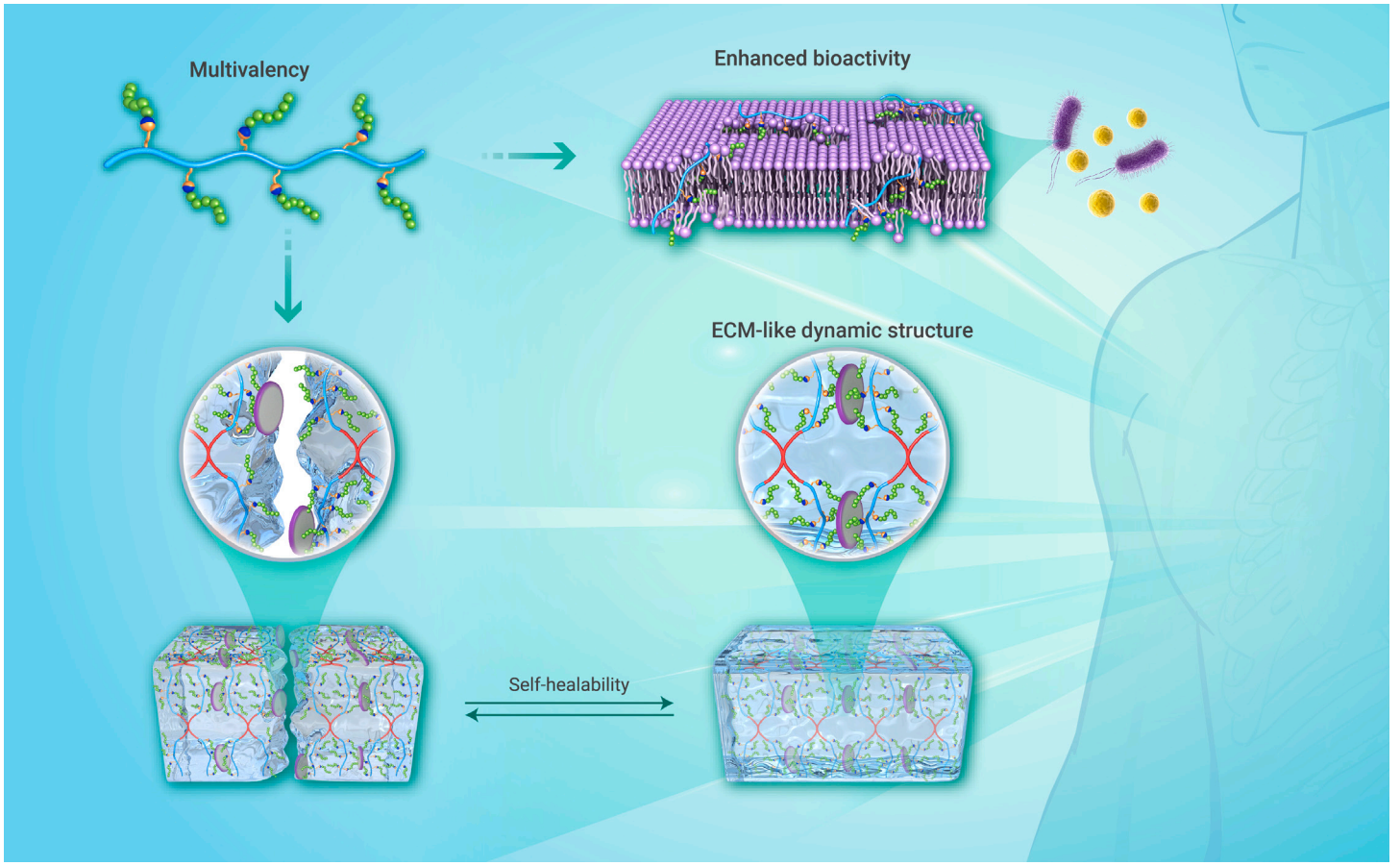

PUBLIC SUMMARY

- The multivalent bioligands that are ubiquitous in biosystems can be rationally designed via precision chemistries.
- Multivalency construction based on antimicrobial peptides leads to enhanced membrane disturbance and bactericidal amplification effects.
- The electrostatic interacting pairs in multivalent antimicrobial peptides enable the fabrication of hydrogels with dynamic structures.
- The multivalent antimicrobial peptide presented here and its hydrogel both demonstrate great potential for the treatment of infected wounds.

REPORT

Rational multivalency construction enables bactericidal effect amplification and dynamic biomaterial design

Xu Chen,[1] Xinrui Li,[1] Wenbo He,[1] Miao Wang,[1] Ang Gao,[2] Liping Tong,[2,*] Shun Guo,[1] Huaiyu Wang,[2,*] and Guoqing Pan[1,*]

[1]Institute for Advanced Materials, School of Materials Science and Engineering, Jiangsu University, Zhenjiang 212013, China

[2]Institute of Biomedicine and Biotechnology, Shenzhen Institute of Advanced Technology, Chinese Academy of Sciences, Shenzhen 518055, China

*Correspondence: lp.tong@siat.ac.cn (L.T.); hy.wang1@siat.ac.cn (H.W.); panguoqing@ujs.edu.cn (G.P.)

Received: March 17, 2023; Accepted: July 10, 2023; Published Online: July 13, 2023; https://doi.org/10.1016/j.xinn.2023.100483

Citation: Chen X., Li X., He W., et al., (2023). Rational multivalency construction enables bactericidal effect amplification and dynamic biomaterial design. The Innovation **4(5)**, 100483.

The multivalency of bioligands in living systems brings inspiration for not only the discovery of biological mechanisms but also the design of extracellular matrix (ECM)-mimicking biomaterials. However, designing controllable multivalency construction strategies is still challenging. Herein, we synthesized a series of well-defined multivalent antimicrobial peptide polymers (mAMPs) by clicking ligand molecules onto polymers prepared by reversible addition-fragmentation chain transfer polymerization. The multiple cationic ligands in the mAMPs could enhance the local disturbance of the anionic phospholipid layer of the bacterial membrane through multivalent binding, leading to amplification of the bactericidal effect. In addition to multivalency-enhanced antibacterial activity, mAMPs also enable multivalency-assisted hydrogel fabrication with an ECM-like dynamic structure. The resultant hydrogel with self-healing and injectable properties could be successfully employed as an antibacterial biomaterial scaffold to treat infected skin wounds. The multivalency construction strategy presented in this work provides new ideas for the biomimetic design of highly active and dynamic biomaterials for tissue repair and regeneration.

INTRODUCTION

Multivalency is widely involved in the physiological and pathological processes in life systems.[1,2] These multiple and reversible intermolecular interactions occurring in the microenvironment composed of cells and the extracellular matrix (ECM) are central to diverse biological responses.[3,4] For example, defense against pathogens involves competitive recognition of multiple carbohydrate ligands between pathogenic and mammalian lectins,[1,5] and cell signaling and intracellular cascades are more inclined to be triggered by efficient activation of multiple membrane receptors.[2,6–9] In addition to immune defense and various cell responses, multivalency is also the intrinsic driving force that supports the structural integrity of living organisms.[10] Multivalent interactions in the biomacromolecular network, including proteins, lipids, and polysaccharides, are crucial to the dynamic but stable three-dimensional structures of cells and ECM.[11–13] In brief, multivalency participates in both biochemical and biophysical processes in biosystems. Therefore, the concept of multivalency deserves in-depth exploration. From the perspective of tissue repair and regeneration, multivalency brings inspiration for not only the discovery of certain biological mechanisms but also the design of advanced biomaterials, since multivalent bioactivities (i.e., biochemical cues) and multivalency-supported dynamic structures (i.e., biophysical cues) are both highly desired for ECM-mimicking biomaterials.[11,14–18]

In recent decades, multivalency has been a well-studied new type of molecular strategy that can enhance specific recognition events.[19–23] Synthetic multivalent ligand molecules have been proposed as therapeutic modalities to enhance the neutralization of toxins,[20,24,25] improve the prevention of pathogen infections, and even accelerate tissue regeneration.[5,26–30] Despite their vast prospects, synthetic multivalent systems as bioactive factors or functional biomaterials for biomedical applications are still very rare.[19,31] This could be ascribed to the complexity (i.e., high reactivity that can damage bioactivities) and low controllability (i.e., hard to control the valence number) of traditional chemistries.[32–34] In this context, precise chemical strategies with mild reaction conditions, high selectivity, and controllability are highly desired for multivalency construction.

As the molecular entities of multivalency, multivalent ligand molecules are reminiscent of polymers with multiple or repeating units. Polymerization might be a feasible means to realize bioligand multivalency through side group grafting. Moreover, the past decades have witnessed the great success of controlled radical polymerization (CRP),[35,36] which can easily obtain well-defined linear polymers with controlled repeating units. Thus, CRP may provide a viable solution to improve controllability during multivalency construction. As another kind of precision chemistry, the click reaction (typically based on azido-alkynyl cycloaddition) enables specific, rapid, and thorough molecular conjugation, thus exhibiting great promise in biomolecule-related molecular grafting, modification, and even synthesis.[37,38] Therefore, we propose to construct multivalency by combining the above two precision chemistries, which may synergistically improve the controllability, operability, and reproducibility for the synthesis of multivalent bioligand molecules.

In this work, we reported a precise multivalency construction strategy by clicking ligand molecules onto well-defined polymers. As a proof of concept, an antimicrobial peptide (AMP) was employed as the model ligand for multivalency construction due to its ability to enhance antibacterial activity and improve therapeutic efficiency for tissue infections.[39] Moreover, the charged molecular structures of polymeric AMPs might facilitate the formation of dynamic biomedical hydrogel materials through multiple electrostatic interactions.[40] These two aspects exactly correspond to the biochemical (i.e., multivalent bioactivities) and biophysical (i.e., dynamic multivalent structures) functions of multivalency in biosystems. Herein, we first synthesized a series of well-defined linear polymers with different alkynyl side groups through reversible addition-fragmentation chain transfer (RAFT) polymerization of alkynyl-containing propargyl acrylamide (PA) and hydrophilic 2-hydroxyethyl acrylamide. Subsequently, the alkynyl-containing polymers were clicked with azido-capped AMPs, leading to precisely controlled multivalent AMPs (mAMPs) (Figure 1A, left). The bactericidal amplification effect of the mAMPs was demonstrated both *in vitro* and *in vivo* (Figure 1A, right). In addition, the optimal mAMP was further employed in the design of a dynamic hydrogel through multiple electrostatic interactions (Figure 1B, upper). As an ECM-mimicking dynamic biomaterial, the mAMP-derived hydrogel exhibited self-healing and injectable properties. Furthermore, the hydrogel was used for treating infected open skin wounds due to its inherent antibacterial activity (Figure 1B, lower). Such high adaptability to wound geometry, efficient resistance to stress-induced fragmentation, and enhanced bactericidal effects may facilitate efficient disinfection of injured sites and continuous support during skin wound repair. In summary, the precision strategy presented in this work may provide an efficient means for multivalency construction, and the multivalency-assisted fabrication of ECM-like dynamic biomaterials will also bring new insights for the development of biomimetic scaffolds for tissue engineering and regenerative medicine.

RESULTS

Multivalent polymer synthesis

The alkynyl-capped functional monomer PA was obtained by amidation of acryloyl chloride with propargylamine according to a reported method (Figures S1 and S2A).[41] During RAFT polymerization, the number of PA repeating units was controlled by feeding different ratios of PA and 2-Hydroxyethyl acrylamide (HEAA). The resultant poly(HA-*co*-PA) polymers (named PHA-PPA$_n$, where n is the number of PA repeating units) were then characterized by NMR. The characteristic peaks of alkynyl hydrogen (−*C*≡*CH*, 3.08 ppm), aromatic hydrogen (−C_6H_5, 7.6 ppm and 7.9 ppm), and methine and methylene hydrogens (−*CH*− and −CH_2−, 1.34–1.93 ppm) in the ^{1}H NMR spectra of the PHA-PPA$_n$ polymers (Figure 2A) were clearly observed. According to the yields and quantification detected from the ^{1}H NMR spectra, the number of PA repeating units and molecular weights of the polymers were determined (Table S1). Three polymers, PHA-PPA$_3$, PHA-PPA$_6$ and PHA-PPA$_{10}$, with increasing numbers of alkynyl

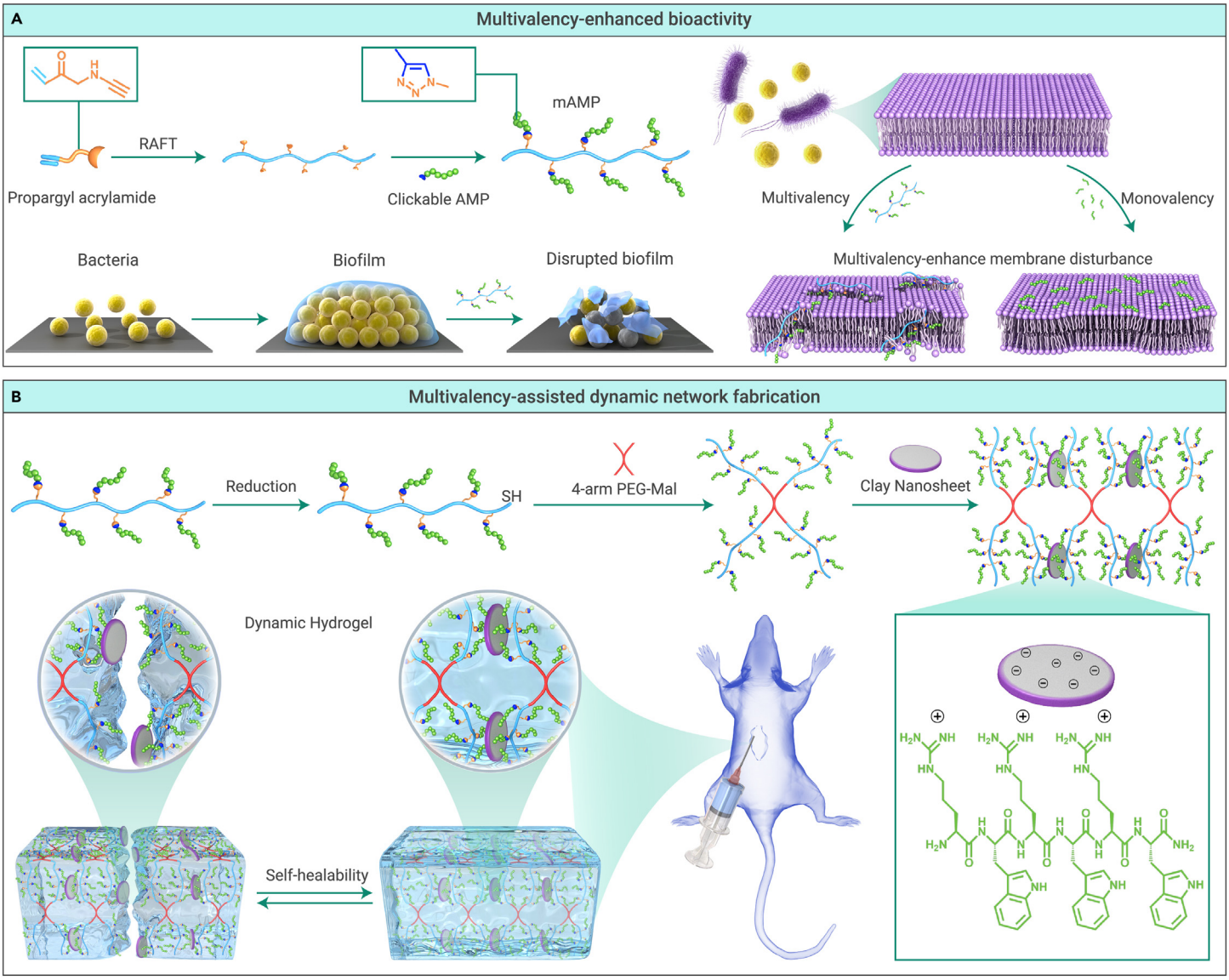

Figure 1. Schematic illustration of the preparation and application of mAMPs and the dynamic hydrogel (A) Synthesis of the mAMP polymers (left) and bactericidal amplification effect of an mAMP through locally enhanced disruption of bacterial membrane lipid bilayers (right). (B) Fabrication of the mAMP-derived dynamic hydrogel through multiple electrostatic interactions with nanoclays (upper) and its application for treating infected open skin wounds (lower).

repeating units but similar chain lengths (polymerization degree of approximately 30) were obtained. Gel permeation chromatography (GPC) confirmed that all three PHA-PPA$_n$ polymers had very similar molecular weights and low polydispersity indices (approximately 1.09–1.17) (Figure 2B), indicating the high controllability of RAFT polymerization for the preparation of multivalent alkynyl polymers.

The three alkynyl polymers (PHA-PPA$_n$) were then clicked by an azido-capped antimicrobial peptide (N_3-RWRWRW) for multivalent molecular construction (Figures S2B–S2D).[42,43] The multivalent AMP polymers (where n is the valence number or repetitive number of AMP) were also characterized by NMR. In comparison to those of PHA-PPA$_n$, the ^{1}H NMR spectra of the mAMP$_n$ samples displayed the characteristic AMP peaks (10.81 ppm and 6.83–7.88 ppm), confirming the successful synthesis of mAMP$_n$ (Figure 2C). The valence number of mAMP$_n$ was further determined (Table S2), and three multivalent AMP polymers, mAMP$_2$, mAMP$_4$ and mAMP$_6$, were obtained, corresponding to the original PHA-PPA$_3$, PHA-PPA$_6$, and PHA-PPA$_{10}$, respectively. Note that the ratio of alkynyl groups that reacted with azido-AMP was only approximately 60%, probably due to steric effects. The above results demonstrated that mAMP$_n$ with precisely controlled multivalent ligands could be efficiently synthesized through the combination of RAFT and click chemistry.

In vitro antibacterial activity

The influence of multivalency on the intrinsic antibacterial activity of the AMP was evaluated. The mAMP$_n$ polymers and free AMP molecules all exhibited concentration-dependent antibacterial activity against gram-negative *Escherichia coli* (Figure 2D). When the concentration AMP increased to 40 μmol L^{-1}, the *E. coli* could be completely killed, indicating a decent bactericidal effect of the monovalent AMP that is consistent with previous studies.[43] In contrast, all the mAMP$_n$ polymers exhibited significantly enhanced bactericidal effects, and the minimum bactericidal concentrations (MBCs) of the mAMP$_n$ polymers against *E. coli* were determined to be approximately 2.5–10 μmol L^{-1} (Figure S3; Table S3). In particular, the MBC of mAMP$_6$ (2.5 μmol L^{-1}) was less than one-tenth of that of the monovalent AMP (40 μmol L^{-1}). Similar results were observed in the tests against gram-positive *Staphylococcus aureus* (Figure 2E). For example, the MBC of the monovalent AMP was 20 μmol L^{-1}, which is about eight times higher than that of mAMP$_6$ (2.5 μmol L^{-1}). In addition, mAMP$_n$ showed faster antibacterial kinetics than the AMP (Figure S4), further indicating the significant effect of mAMP$_n$ polymers to amplify the antibacterial activity.

To more intuitively reveal the antibacterial mechanism,[44] the membrane morphology of the bacteria after treatment was examined by scanning electron microscope (SEM) and transmission electron microscope (TEM) (Figures 2F and 2G). The SEM images showed that the number of bacteria after treatment was

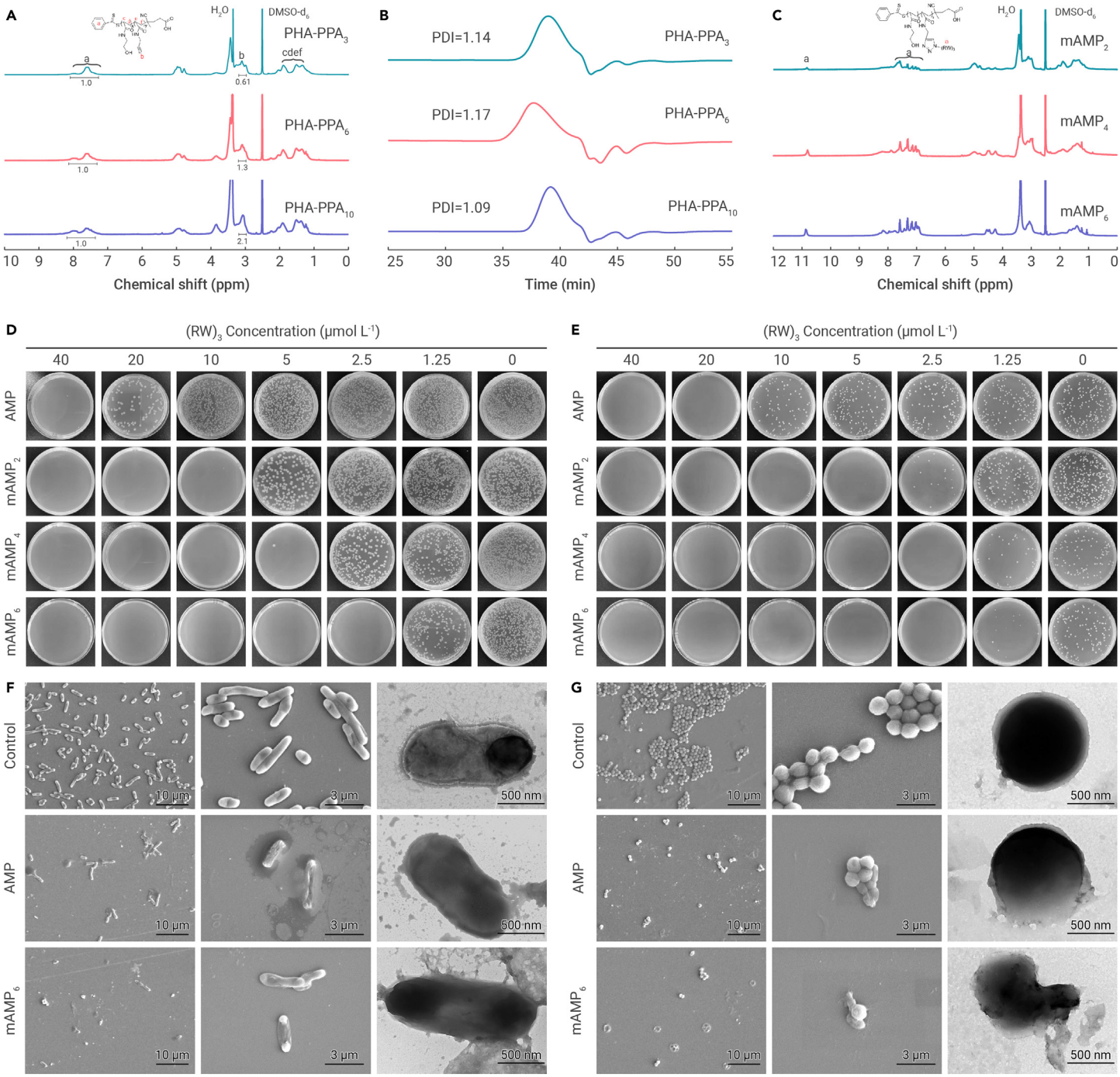

Figure 2. Chemical characterization and antibacterial activities of mAMP$_n$ (A and B) ^{1}H NMR spectra (A) and GPC analysis (B) of PHA-PPA$_n$. (C) ^{1}H NMR spectra of mAMP$_n$. (D and E) Bacterial colony images of *E. coli* (D) and *S. aureus* (E) incubated with various concentrations of AMP and mAMP$_n$ for 8 h. (F and G) SEM (left) and TEM (right) images of *E. coli* (F) and *S. aureus* (G) after 8 h of treatment with AMP and mAMP$_6$ (40 μmol L^{-1}). Data are represented as mean ± SD (n = 4).

significantly reduced, and their morphology mostly showed collapsed and fused states, demonstrating highly efficient destruction of the bacterial cell wall. The TEM images further revealed that the clearly visible membranes on bacteria in the control groups disappeared after treatment with AMP and mAMP$_6$, leaving an incomplete morphology and only a trace of leaked cytoplasmic matrix. We considered that stronger electrostatic binding forces and the ligand confinement of mAMP$_n$ might lead to the locally enhanced membrane distribution compared with that of monovalent AMP, which contributed greatly to the amplification of antibacterial activity.[2]

Multivalent antibacterial mechanism

We speculated that the bactericidal amplification effect of mAMP$_n$ was due to locally enhanced ligand binding of multivalent molecules (Figure 3A). To verify this hypothesis, the binding of AMP and mAMP$_n$ to bacteria was investigated by confocal laser scanning microscopy (CLSM). After incubation with fluorescein isothiocyanate (FITC)-labeled AMP and mAMP$_n$ (Tables S4 and S5) for 20 min, we found that the green fluorescence from FITC that appeared on the mAMP$_6$-treated bacteria was significantly stronger than that on the AMP-treated bacteria (Figures 3B and S5). Quantitative analysis showed that the bacterial binding rates for the AMP and the mAMP$_6$ polymers were 22.9% and 51.9%, respectively (Figure 3C). The quartz crystal microbalance (QCM) tests confirmed this result. The significantly decreased frequency (*f*) after solution injection more intuitively demonstrated the stronger binding action and confirmed the multivalency-enhanced ligand binding of the mAMP$_6$ polymer on bacterial membranes (Figures 3D and 3E). Therefore, the local ligand concentration and the binding force of mAMP$_n$ on the bacterial membrane are much higher, which could

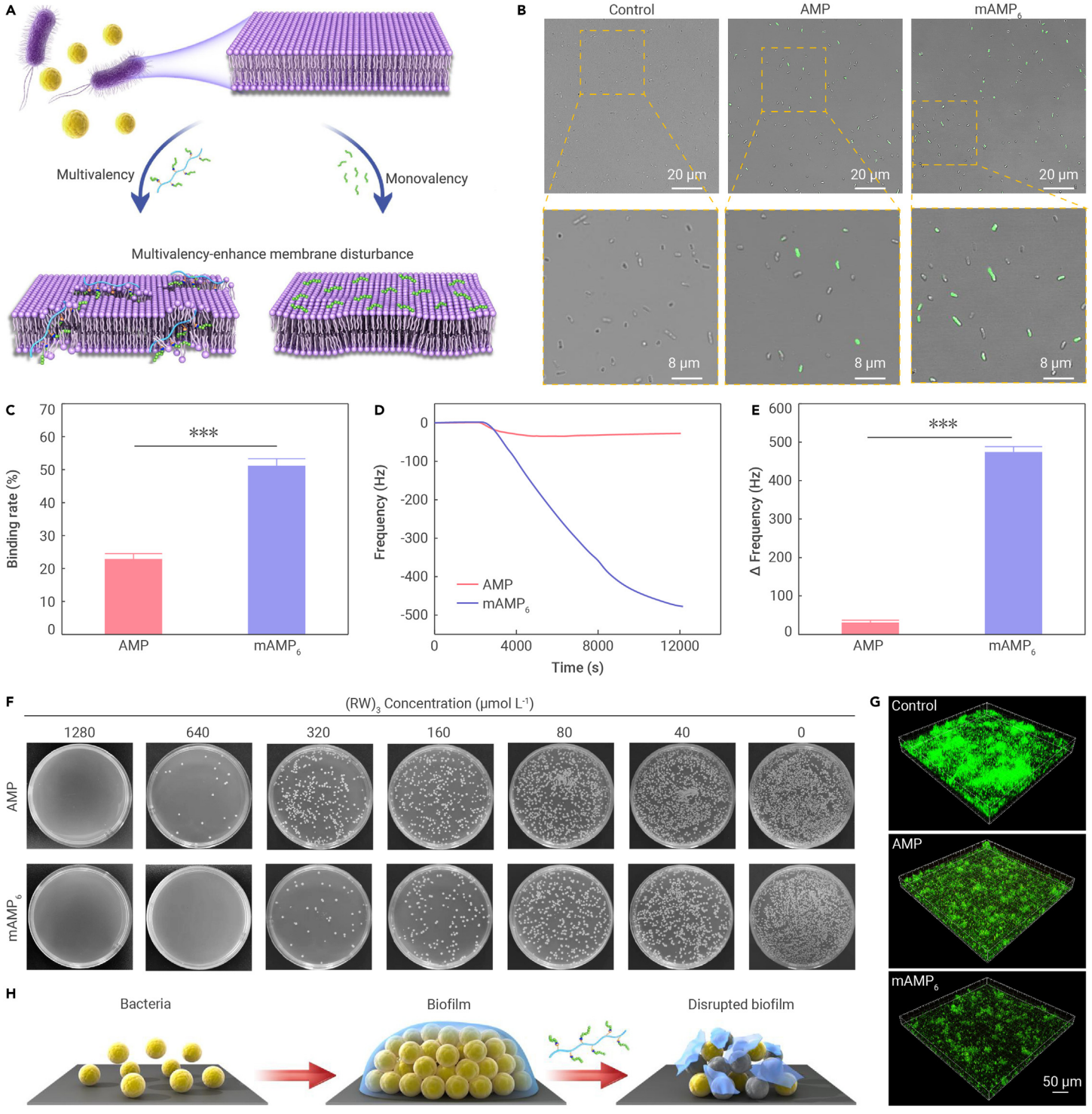

Figure 3. The enhanced antibacterial mechanism of $mAMP_n$ (A) Schematic illustration of the bactericidal amplification effect provided by $mAMP_n$. (B and C) CLSM images (B) and quantitative analysis (C) of the binding of FITC-labeled AMP or $mAMP_6$ to bacteria. (D) Real-time QCM frequency changes during binding of AMP or $mAMP_6$ (40 μmol L^{-1}). (E) Quantitative results of frequency changes. (F) Efficiency of *S. aureus* biofilm eradication after treatment with AMP and $mAMP_6$ for 8 h. (G) CLSM images of *S. aureus* biofilms after treatment (640 μmol L^{-1}). (H) Schematic illustration of biofilm eradication using multivalent polymers. Data are represented as mean ± SD (n = 4); a statistically significant difference compared with the control group is indicated by ***$p < 0.001$.

significantly enhance the disturbance of the anionic phospholipid layer, thus exhibiting amplified bactericidal effects.

Biofilm inhibition

In the clinic, bacterial biofilms in chronic wound infections are extremely difficult to cure.[45,46] Thus, we attempted to apply the multivalent antibacterial polymer to eliminate biofilms. As shown in Figure 3F, the minimum eradication biofilm concentrations of AMP and $mAMP_6$ were determined to be 1,280 and 640 μmol L^{-1}, respectively. Live/dead staining showed that the original dense biofilm was significantly reduced after $mAMP_6$ treatment for 8 h, and the surface became sparse and irregular (Figure 3G). Therefore, we have a preliminary inference that multivalent binding could accelerate the permeation and removal of the protective layer of the biofilm (e.g., extracellular polymeric substances), thus exposing the inner bacteria.[47,48] After losing its barrier function, the damaged biofilm could be easily penetrated by $mAMP_6$ polymers, leading to an improved biofilm eradication efficiency (Figure 3H).

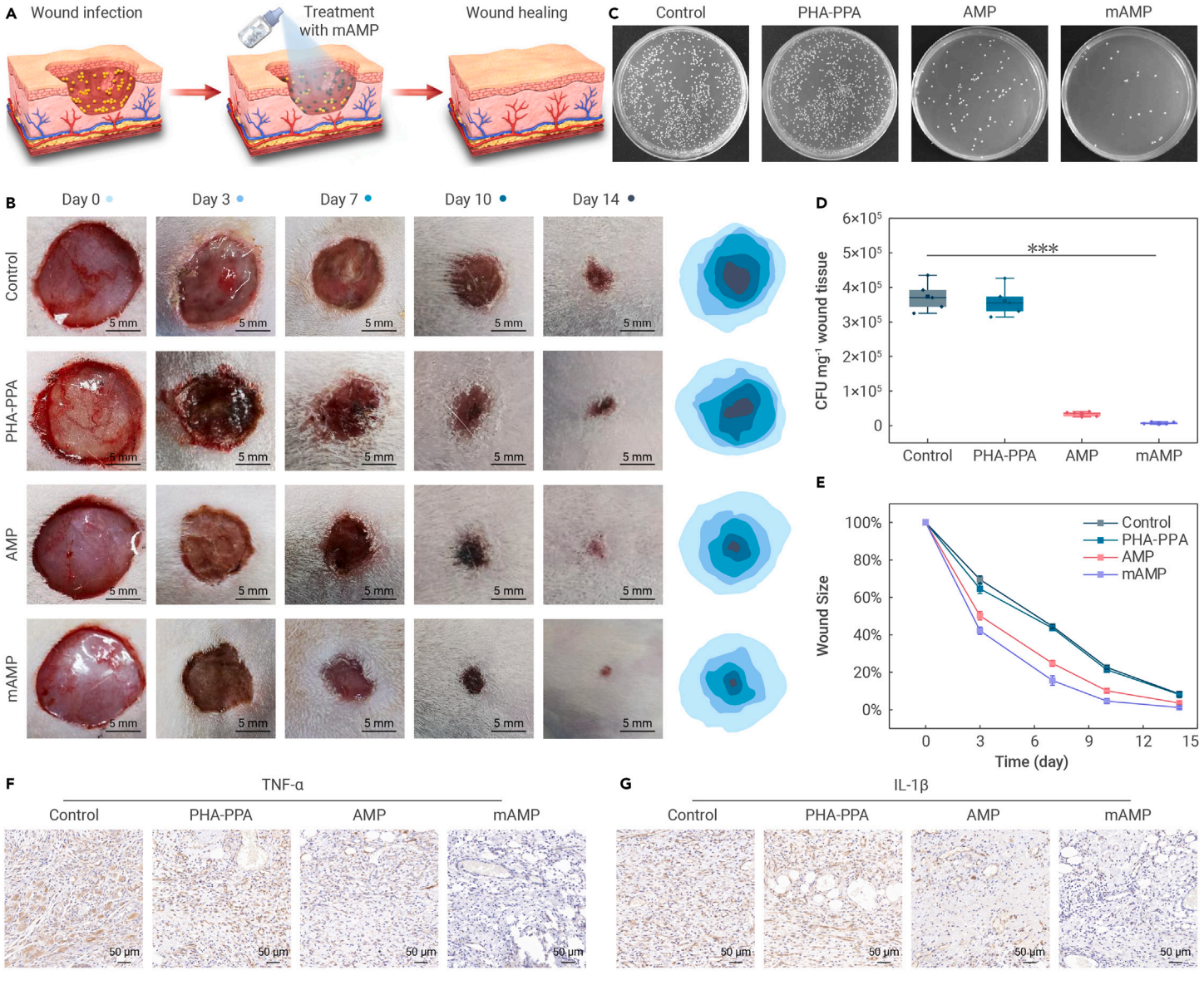

Figure 4. ***In vivo* antibacterial activity of mAMP$_n$** (A) Skin wound model for the *in vivo* anti-infection assay. (B) Wound healing processes in different groups of rats. (C and D) Images (C) and quantitative analysis (D) of the bacterial colonies obtained from the wound sites on day 3. (E) Quantitative analysis of wound sizes. (F and G) Immunofluorescence staining of TNF-α (F) and IL-1β (G) in the wound site on day 7. Data are represented as mean ± SD (n = 5); a statistically significant difference compared with the control group is indicated by ***p < 0.001.

Biocompatibility

Both AMP and mAMP$_n$ exhibited very low hemolytic toxicity, which was almost negligible at concentrations below 10 μmol L^{-1} (Figures S6A–S6C). Thus, the mAMP$_6$ polymer could be considered to have no hemolytic toxicity in its effective antibacterial concentration ranges (2.5–10 μmol L^{-1}). In addition to hemolytic toxicity, the cytotoxicity of mAMP$_n$ was also determined with live/dead staining. As expected, treated mouse fibroblast (L929) cells showed only very few red dead cells (Figure S6D). Moreover, the treated cells could be recovered and exhibited perfect proliferative ability (Figure S6E). The above results indicated the excellent biocompatibility of the mAMP$_n$ polymers.

In vivo anti-infective ability

We then established an *S. aureus*-infected skin wound model in rats to investigate the *in vivo* anti-infective potential of mAMP$_n$ (Figure 4A). The anti-infection and wound healing processes were then evaluated (Figure 4B). In the early stages, yellow pus was clearly found on the infected wound bed in the PBS and PH-PPA groups, indicating the severity of infection. However, such pyogenic infection was not observed in the AMP and mAMP$_6$ groups, which was also confirmed by the agar plate count method of tissue exudate from the wound sites (Figures 4C and 4D). In addition to stronger anti-infection properties, the mAMP$_6$-treated wounds exhibited the fastest wound closure rate over 14 days, probably due to the faster elimination of bacteria *in vivo* and the initiation of the tissue reconstruction process (Figure 4E). Hematoxylin and eosin (H&E) and Masson's trichrome staining were also used to examine the anti-infection and wound healing efficacy. The skin defects in the mAMP$_6$ group were completely closed with highly regular epithelium, numerous hair follicles (green arrows), and almost complete regeneration of the dermal tissue (improved granulation length and collagen deposition) on day 14 (Figure S7). The infection-induced inflammatory responses were also examined (Figures 4F and 4G). Two typical proinflammatory cytokines,[49,50] tumor necrosis factor alpha (TNF-α) and interleukin-1β (IL-1β), were highly expressed on day 7 in the other groups in contrast to their significantly reduced expression in the mAMP$_6$ group. These results together demonstrated the promise of mAMP$_6$ as an antibacterial therapeutic for treating *in vivo* bacterial infections and improving wound healing.

Dynamic hydrogel fabrication

We further used the multivalent mAMP$_n$ polymer to fabricate an ECM-like biomaterial with a dynamic structure. The mAMP$_6$ polymer was successfully linked onto four-armed poly(ethylene glycol) (4-arm-PEG) through thiol reduction and Michael addition reactions (Figures 5A and S8). Due to the multiple

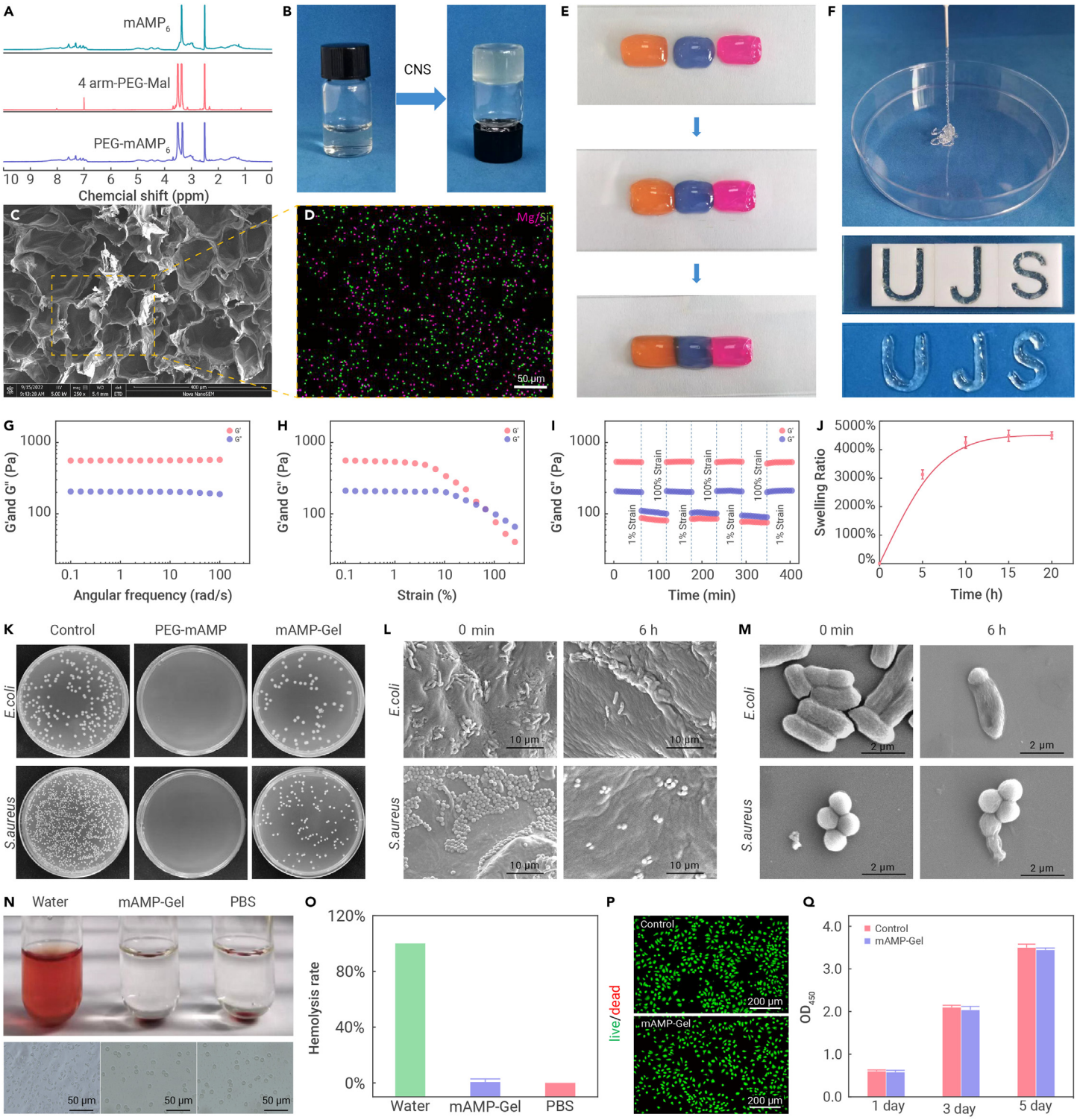

Figure 5. Characterization of the mAMP-Gel (A) ^{1}H NMR spectra. (B) Gelation of mAMP-Gel. (C) SEM image of mAMP-Gel. (D) EDS mapping image of mAMP-Gel (red, Mg; green, Si). (E) The self-healing ability of mAMP-Gel. Block sizes: 0.2 × 0.5 cm. (F) The injectability and remoldability of mAMP-Gel. Teflon molds: 2.0 × 2.0 cm. (G) Dynamic oscillatory frequency sweeps (strain = 1%) of mAMP-Gel. (H) Strain amplitude sweeps (γ = 66%) of mAMP-Gel. (I) Continuous step strain sweep (strain = 1 or 100%) of mAMP-Gel. Temperature: 25°C. (J) The swelling properties of mAMP-Gel. (K) Images of bacterial colonies treated with PEG-mAMP and mAMP-Gel for 12 h. (L and M) SEM images of bacteria seeded on mAMP-Gel for 6 h. (N and O) Hemolytic photos (N) and hemolysis rates (O) after 2 h of treatment with mAMP-Gel. (P and Q) Live/dead staining images (P) and proliferation profiles (Q) of L929 cells incubated with mAMP-Gel. Data are represented as mean ± SD (n = 4).

guanidinium groups, the PEG-mAMP$_6$ polymer could be rapidly crosslinked by clay nanosheets (CNSs) through multiple electrostatic interactions (Figures 5B, 5D, and S9).[51,52] The porous structure of the hydrogel (mAMP-Gel) also implied its potential as a biomaterial to support cell growth in tissue engineering (Figure 5C).

Due to the reversibility of multiple electrostatic interactions, we expect the mAMP-Gel to display typical dynamic properties, such as self-healing ability, remoldability, and injectability.[53] As shown in Figure 5E, the cut hydrogel blocks healed within 30 min and integrated together even after the application of a certain tensile force. In addition, mAMP-Gel has excellent injectable properties due to its shear thinning behavior (Figure 5F and Video S1). Rheological tests were further performed to examine the dynamic mechanism of mAMP-Gel.[54] Dynamic oscillatory sweep tests revealed that the hydrogel storage modulus (G') was higher than the loss modulus (G''), indicating its elastic gel-like properties

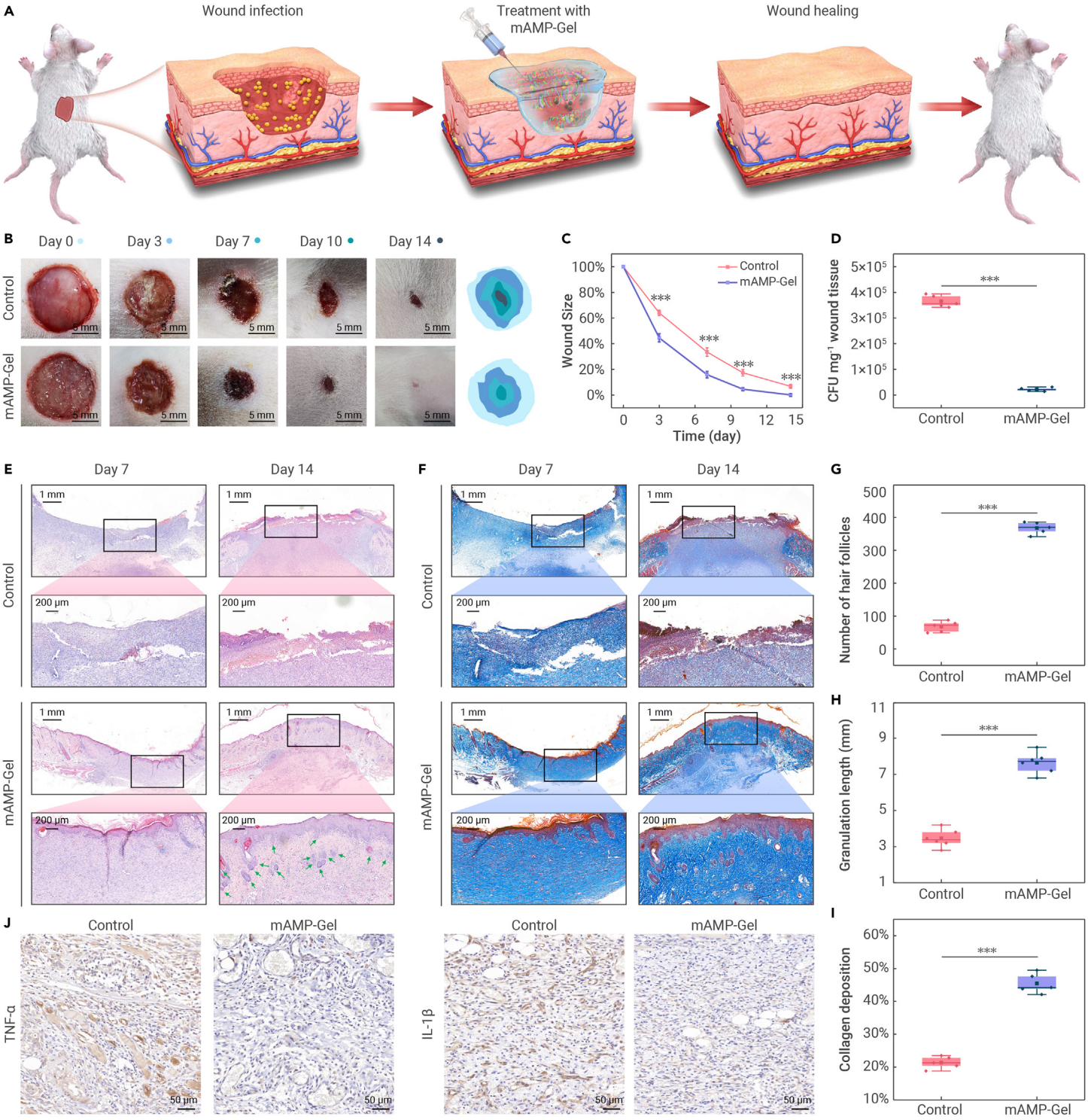

Figure 6. ***In vivo*** **antibacterial activity of mAMP-Gel** (A) Schematic illustration of the treatment and healing of infected skin wounds after injection of mAMP-Gel. (B and C) Wound healing processes (B) and changes in wound sizes (C) in different groups. (D) Quantitative analysis of the number of bacterial colonies obtained from the wound tissues of different groups on day 3. (E and F) H&E (E) and Masson's trichrome (F) staining of the skin wound tissues harvested from different groups on days 7 and 14. Green arrows indicate the hair follicles. (G–I) Quantification of the number of hair follicles (G), granulation length (H), and collagen deposition (I) in different groups on day 14. (J) Immunofluorescence staining of TNF-α and IL-1β in different groups on day 7. Data are represented as mean ± SD (n = 5); a statistically significant difference compared with the control group is indicated by ***$p < 0.001$.

(Figure 5G). As shown in Figure 5H, the strain sweeps indicated that the hydrogels had a typical elastic response. The value of G′ decreased rapidly to below that of G″ above the critical strain region (γ = 66%), indicating a collapse of the gel to the sol state. We further found that the hydrogel very rapidly recovered its mechanical properties when it was applied with an alternating strain between 1% and 100% (Figure 5I). In addition, after repeated alternating strain sweeps, the values of G′ and G″ recovered to their initial values, further confirming the dynamic but stable structure of mAMP-Gel. The above tests demonstrated the dynamic structure and mechanism of mAMP-Gel.

Since dynamic hydrogels possess great potential in biomedicine, some critical parameters (swelling rate, degradation rate, antibacterial activity, and biocompatibility) of the resultant mAMP-Gel were further studied. We found that mAMP-Gel exhibited excellent swelling properties and was almost completely degraded within 2 weeks *in vitro* (Figures 5J and S10). Note that the antibacterial activity

of mAMP-Gel was slightly compromised during the hydrogel formation process,[55] probably due to sterics restricting the contact between the AMP ligand and bacteria (Figures 5K and S11). Nevertheless, bacteria could be completely killed by mAMP-Gel after an extended incubation time. PEG-mAMP$_6$ also still exhibited excellent antibacterial properties. The number of bacteria after treatment was significantly reduced after 6 h, and the residual bacteria mostly showed collapsed and fused states (Figures 5L and 5M). It is also worth mentioning that the dynamic mAMP-Gel exhibited excellent biocompatibility. In addition to negligible hemolytic toxicity (Figures 5N and 5O), cells cocultured with the dynamic hydrogel maintained high viability for 12 h (Figures 5P and S12), and their proliferation rate was nearly equivalent to that of the cells in the control group without treatment (Figure 5Q). The above results implied the great potential of this dynamic mAMP-Gel hydrogel for use as a biocompatible and anti-infective scaffold biomaterial, particularly for the treatment and repair of infection-prone tissues.

Using the dynamic hydrogel as a wound dressing

With this dynamic antibacterial hydrogel in hand, we further established a full-thickness infected wound model on rat skin to investigate the potential of the hydrogel as an advanced wound dressing material for infected skin repair and regeneration (Figure 6A). Two different groups, treated with PBS (control) or with the dynamic mAMP-Gel, were used to evaluate wound healing efficacy. As shown in Figure 6B, great suppuration was observed on the infected wound bed in the control group on day 3, indicating the severity of wound infection. In contrast, such pyogenic phenomena were never observed in the group injected with mAMP-Gel hydrogel, suggesting that mAMP-Gel treatment could effectively kill bacteria and inhibit infection. Re-culture of the wound exudate on agar plates confirmed that there were significantly fewer bacteria in the mAMP-Gel group on day 3 (Figures 6D and S13), verifying the efficient anti-infective ability of the hydrogel. Due to the rapid elimination of bacteria, the tissue reconstruction process in the mAMP-Gel group was initiated in a timely manner, and the wounds in this group healed within 14 days (Figure 6C). However, no wounds in the control group healed completely within the same period.

H&E and Masson's trichrome staining were further employed to evaluate tissue healing efficacy. As shown in Figures 6E and 6F, the skin defects in the mAMP-Gel group were almost closed with a highly regular epithelium, numerous hair follicles, extensive collagen deposition, and almost complete regeneration of dermal tissue on day 14. In contrast, epithelialization in the control group was incomplete, and a large area of immature granulation tissue was deposited around the wound. Quantitative analysis showed that the number of hair follicles, granulation length, and collagen deposition were significantly improved in the mAMP-Gel group (Figures 6G–6I). Moreover, the expression levels of TNF-α and IL-1β were also significantly reduced due to the anti-infection ability of mAMP-Gel, which could significantly reduce inflammatory responses (Figure 6J). Finally, histological assessment of major organs (e.g., heart, liver, spleen, lung, and kidney) was performed to examine the long-term biosafety of the mAMP-Gel hydrogel (Figure S14). Similar to the control group, no obvious lesions or other histopathological abnormalities were observed in tissue sections in the mAMP-Gel group.

Although the *in vivo* anti-infection abilities of the mAMP polymer and mAMP-Gel were not significantly different, the superiority of mAMP-Gel during the wound repair stage was clear. Infected wounds treated with mAMP-Gel healed and had a better tissue structure (Figures 4B and 6B). The H&E staining images revealed that although the wounds in both the mAMP polymer group and mAMP-Gel group could completely epithelialize in 14 days, the epithelial layer in the mAMP-Gel group was notably more regular and thicker. In addition, some elongated hair follicles grew in the mAMP-Gel group (Figures S7 and S6E). This is probably due to the protective effect of the hydrogel, which can provide structural support and keep the wound moist, thus facilitating the growth and migration of endothelial cells and fibroblasts.[56] The above positive results clearly demonstrated that the multivalency-supported dynamic hydrogel might be used as a biocompatible, easy to handle, and antibacterial scaffold material for infected tissue repair and regeneration.

CONCLUSION

In summary, we herein reported a precise strategy to construct multivalency by combining controlled polymerization and click chemistry and then applied the generated multivalent molecules to fabricate dynamic biomaterials. We first synthesized a series of well-defined linear polymers with different alkynyl side groups through RAFT polymerization. Subsequently, the alkynyl polymers were clicked with azido-AMP to obtain precisely controlled multivalent AMP polymers (mAMPs). Due to the aggregation of cationic AMP ligands and locally enhanced disturbance of the bacterial membrane, the mAMPs significantly amplified the bactericidal effect (8- to about 10-fold). The mAMPs were further employed for dynamic crosslinking with negatively charged CNSs via multiple electrostatic interactions. As an ECM-like dynamic biomaterial, the mAMP-derived hydrogel exhibited typical dynamic properties, including self-healing ability, injectability and remoldability. Furthermore, this hydrogel could be used for treating infected open skin wounds due to its inherent antibacterial activity. The high adaptability to wound geometry, efficient resistance to stress-induced fragmentation, and enhanced bactericidal effect enabled the dynamic hydrogel to efficiently disinfect infected sites and continuously support skin wound repair *in vivo*. In summary, the precision chemistries used in this study may provide an efficient means for multivalency construction, and the multivalency-assisted fabrication of ECM-mimicking dynamic hydrogels will also provide new insights for the biomimetic design of dynamic and highly bioactive materials in tissue engineering and regenerative medicine.

MATERIAL AND METHODS

See supplemental information for details.

REFERENCES

1. Fasting, C., Schalley, C.A., Weber, M., et al. (2012). Multivalency as a chemical organization and action principle. Angew. Chem. Int. Ed. ***51***, 10472–10498.
2. Mammen, M., Choi, S.-K., and Whitesides, G.M. (1998). Polyvalent interactions in biological systems: Implications for design and use of multivalent ligands and inhibitors. Angew. Chem. Int. Ed. ***37***, 2754–2794.
3. Kitov, P.I., and Bundle, D.R. (2003). On the nature of the multivalency effect: A thermodynamic model. J. Am. Chem. Soc. ***125***, 16271–16284.
4. Lundquist, J.J., and Toone, E.J. (2002). The cluster glycoside effect. Chem. Rev. ***102***, 555–578.
5. Liu, S.P., Zhou, L., Lakshminarayanan, R., et al. (2010). Multivalent antimicrobial peptides as therapeutics: Design principles and structural diversities. Int. J. Pept. Res. Therapeut. ***16***, 199–213.
6. Kiessling, L.L., Gestwicki, J.E., and Strong, L.E. (2000). Synthetic multivalent ligands in the exploration of cell-surface interactions. Curr. Opin. Chem. Biol. ***4***, 696–703.
7. Haudenschild, D.R., Hong, E., Yik, J.H.N., et al. (2011). Enhanced activity of transforming growth factor β1 (tgf-β1) bound to cartilage oligomeric matrix protein. J. Biol. Chem. ***286***, 43250–43258.
8. Holler, N., Tardivel, A., Kovacsovics-Bankowski, M., et al. (2003). Two adjacent trimeric fas ligands are required for fas signaling and formation of a death-inducing signaling complex. Mol. Cell Biol. ***23***, 1428–1440.
9. Ye, S., Luo, Y., Lu, W., et al. (2001). Structural basis for interaction of fgf-1, fgf-2, and fgf-7 with different heparan sulfate motifs. Biochemistry ***40***, 14429–14439.
10. Perris, R., and Perissinotto, D. (2000). Role of the extracellular matrix during neural crest cell migration. Mech. Dev. ***95***, 3–21.
11. Hynes, R.O. (2009). The extracellular matrix: Not just pretty fibrils. Science ***326***, 1216–1219.
12. Frantz, C., Stewart, K.M., and Weaver, V.M. (2010). The extracellular matrix at a glance. J. Cell Sci. ***123***, 4195–4200.
13. Nakamura, H., Lee, A.A., Afshar, A.S., et al. (2018). Intracellular production of hydrogels and synthetic rna granules by multivalent molecular interactions. Nat. Mater. ***17***, 79–89.
14. He, W., Wang, Q., Tian, X., et al. (2022). Recapitulating dynamic ecm ligand presentation at biomaterial interfaces: Molecular strategies and biomedical prospects. Exploration ***2***, 20210093.
15. Ma, Y., Tian, X., Liu, L., et al. (2019). Dynamic synthetic biointerfaces: From reversible chemical interactions to tunable biological effects. Acc. Chem. Res. ***52***, 1611–1622.
16. Tong, Z., Jin, L., Oliveira, J.M., et al. (2021). Adaptable hydrogel with reversible linkages for regenerative medicine: Dynamic mechanical microenvironment for cells. Bioact. Mater. ***6***, 1375–1387.
17. Rosales, A.M., and Anseth, K.S. (2016). The design of reversible hydrogels to capture extracellular matrix dynamics. Nat. Rev. Mater. ***1***, 15012–15015.
18. He, W., Bai, J., Chen, X., et al. (2022). Reversible dougong structured receptor–ligand recognition for building dynamic extracellular matrix mimics. Proc. Natl. Acad. Sci. USA ***119***, e2117221119.
19. Compain, P., and Bodlenner, A. (2014). The multivalent effect in glycosidase inhibition: A new, rapidly emerging topic in glycoscience. Chembiochem ***15***, 1239–1251.
20. Kanfar, N., Bartolami, E., Zelli, R., et al. (2015). Emerging trends in enzyme inhibition by multivalent nanoconstructs. Org. Biomol. Chem. ***13***, 9894–9906.
21. Morzy, D., and Bastings, M. (2022). Significance of receptor mobility in multivalent binding on lipid membranes. Angew. Chem. Int. Ed. ***61***, e202114167.

22. Weissleder, R., Kelly, K., Sun, E.Y., et al. (2005). Cell-specific targeting of nanoparticles by multivalent attachment of small molecules. Nat. Biotechnol. ***23***, 1418–1423.
23. González-Cuesta, M., Ortiz Mellet, C., and García Fernández, J.M. (2020). Carbohydrate supramolecular chemistry: Beyond the multivalent effect. Chem. Commun. ***56***, 5207–5222.
24. St Hilaire, P.M., Boyd, M.K., and Toone, E.J. (1994). Interaction of the shiga-like toxin type 1 b-subunit with its carbohydrate receptor. Biochemistry ***33***, 14452–14463.
25. Vance, D., Shah, M., Joshi, A., et al. (2008). Polyvalency: A promising strategy for drug design. Biotechnol. Bioeng. ***101***, 429–434.
26. Von Itzstein, M., Wu, W.-Y., Kok, G.B., et al. (1993). Rational design of potent sialidase-based inhibitors of influenza virus replication. Nature ***363***, 418–423.
27. Sigal, G.B., Mammen, M., Dahmann, G., et al. (1996). Polyacrylamides bearing pendant α-sialoside groups strongly inhibit agglutination of erythrocytes by influenza virus: The strong inhibition reflects enhanced binding through cooperative polyvalent interactions. J. Am. Chem. Soc. ***118***, 3789–3800.
28. Cuellar-Camacho, J.L., Bhatia, S., Reiter-Scherer, V., et al. (2020). Quantification of multivalent interactions between sialic acid and influenza a virus spike proteins by single-molecule force spectroscopy. J. Am. Chem. Soc. ***142***, 12181–12192.
29. Conway, A., Vazin, T., Spelke, D.P., et al. (2013). Multivalent ligands control stem cell behaviour *in vitro* and *in vivo*. Nat. Nanotechnol. ***8***, 831–838.
30. Kaur, G., Wang, C., Sun, J., et al. (2010). The synergistic effects of multivalent ligand display and nanotopography on osteogenic differentiation of rat bone marrow stem cells. Biomaterials ***31***, 5813–5824.
31. Englund, E.A., Wang, D., Fujigaki, H., et al. (2012). Programmable multivalent display of receptor ligands using peptide nucleic acid nanoscaffolds. Nat. Commun. ***3***, 614.
32. Yang, Z., Zhao, X., Hao, R., et al. (2020). Bioclickable and mussel adhesive peptide mimics for engineering vascular stent surfaces. Proc. Natl. Acad. Sci. USA ***117***, 16127–16137.
33. Xiao, Y., Wang, W., Tian, X., et al. (2020). A versatile surface bioengineering strategy based on mussel-inspired and bioclickable peptide mimic. Research ***2020***, 7236946.
34. Chen, X., Gao, Y., Wang, Y., et al. (2021). Mussel-inspired peptide mimicking: An emerging strategy for surface bioengineering of medical implants. Smart Mater. Med. ***2***, 26–37.
35. Parkatzidis, K., Wang, H.S., Truong, N.P., et al. (2020). Recent developments and future challenges in controlled radical polymerization: A 2020 update. Chem ***6***, 1575–1588.
36. Boyer, C., Bulmus, V., Davis, T.P., et al. (2009). Bioapplications of raft polymerization. Chem. Rev. ***109***, 5402–5436.
37. Moses, J.E., and Moorhouse, A.D. (2007). The growing applications of click chemistry. Chem. Soc. Rev. ***36***, 1249–1262.
38. Xi, W., Scott, T.F., Kloxin, C.J., et al. (2014). Click chemistry in materials science. Adv. Funct. Mater. ***24***, 2572–2590.
39. Gidalevitz, D., Ishitsuka, Y., Muresan, A.S., et al. (2003). Interaction of antimicrobial peptide protegrin with biomembranes. Proc. Natl. Acad. Sci. USA ***100***, 6302–6307.
40. Reddy, K.V.R., Yedery, R.D., and Aranha, C. (2004). Antimicrobial peptides: Premises and promises. Int. J. Antimicrob. Agents ***24***, 536–547.
41. Wipf, P., Aoyama, Y., and Benedum, T.E. (2004). A practical method for oxazole synthesis by cycloisomerization of propargyl amides. Org. Lett. ***6***, 3593–3595.
42. Strøm, M.B., Haug, B.E., Skar, M.L., et al. (2003). The pharmacophore of short cationic antibacterial peptides. J. Med. Chem. ***46***, 1567–1570.
43. Liu, Z., Brady, A., Young, A., et al. (2007). Length effects in antimicrobial peptides of the (rw) n series. Antimicrob. Agents Chemother. ***51***, 597–603.
44. Silva, J.P., Appelberg, R., and Gama, F.M. (2016). Antimicrobial peptides as novel anti-tuberculosis therapeutics. Biotechnol. Adv. ***34***, 924–940.
45. Darvishi, S., Tavakoli, S., Kharaziha, M., et al. (2022). Advances in the sensing and treatment of wound biofilms. Angew. Chem. Int. Ed. ***61***, e202112218.
46. Sun, J., Li, M., Lin, M., et al. (2021). High antibacterial activity and selectivity of the versatile polysulfoniums that combat drug resistance. Adv. Mater. ***33***, 2104402.
47. Blackman, L.D., Qu, Y., Cass, P., et al. (2021). Approaches for the inhibition and elimination of microbial biofilms using macromolecular agents. Chem. Soc. Rev. ***50***, 1587–1616.
48. Flemming, H.-C., and Wingender, J. (2010). The biofilm matrix. Nat. Rev. Microbiol. ***8***, 623–633.
49. Fan, X., Yang, F., Huang, J., et al. (2019). Metal–organic-framework-derived 2d carbon nanosheets for localized multiple bacterial eradication and augmented anti-infective therapy. Nano Lett. ***19***, 5885–5896.
50. Gonzalez, A., Sahaza, J.H., Ortiz, B.L., et al. (2003). Production of pro-inflammatory cytokines during the early stages of experimental paracoccidioides brasiliensis infection. Med. Mycol. ***41***, 391–399.
51. Wang, Q., Mynar, J.L., Yoshida, M., et al. (2010). High-water-content mouldable hydrogels by mixing clay and a dendritic molecular binder. Nature ***463***, 339–343.
52. Tamesue, S., Ohtani, M., Yamada, K., et al. (2013). Linear versus dendritic molecular binders for hydrogel network formation with clay nanosheets: Studies with aba triblock copolyethers carrying guanidinium ion pendants. J. Am. Chem. Soc. ***135***, 15650–15655.
53. Ma, Y., He, P., Xie, W., et al. (2021). Dynamic colloidal photonic crystal hydrogels with self-recovery and injectability. Research ***2021***, 9565402.
54. Yin, W., Wang, Q., Zhang, J., et al. (2022). A dynamic nano-coordination protein hydrogel for photothermal treatment and repair of infected skin injury. J. Mater. Chem. B ***10***, 8181–8185.
55. Imura, Y., Nishida, M., and Matsuzaki, K. (2007). Action mechanism of pegylated magainin 2 analogue peptide. Biochim. Biophys. Acta ***1768***, 2578–2585.
56. Murakami, K., Aoki, H., Nakamura, S., et al. (2010). Hydrogel blends of chitin/chitosan, fucoidan and alginate as healing-impaired wound dressings. Biomaterials ***31***, 83–90.

ACKNOWLEDGMENTS

We acknowledge the National Natural Science Foundation of China (32222041, 21875092 and 82272157), the National Natural Science Foundation of Jiangsu Province (BK20220059), the National Key Research and Development Program of China (2019YFA0112000), the Innovation and Entrepreneurship Program of Jiangsu Province, and the "Jiangsu Specially-Appointed Professor" Program.

AUTHOR CONTRIBUTIONS

X.C., L.T., H.W., and G.P. conceived the idea and designed the experiments. G.P. supervised the project. X.C., X.L., and W.H. carried out the experiments. X.C. and G.P. analyzed the data with the help of M.W., A.G., and S.G. X.C., H.W., and G.P. wrote the manuscript.

DECLARATION OF INTERESTS

The authors declare no competing interests.

SUPPLEMENTAL INFORMATION

It can be found online at https://doi.org/10.1016/j.xinn.2023.100483.

LEAD CONTACT WEBSITE

http://faculty.ujs.edu.cn/panguoqing/zh_CN/index.htm.